Molecular Tribology

Friction, wear and adhesion, the three major aspects of *Tribology* play an important role in mankind's efforts to conserve energy. Friction and drag alone account for about one third of the energy needed to run our machines in the industrialized World. This does not account for energy losses due to consequential wear and failure of equipment. It is argued that about 1-2 percent of the GDP could be recovered with appropriate tribological solutions that entail besides liquid phase lubrication also effective solid phase solutions. The challenge is still to connect rational molecular designs to the phenomenological process parameters that attempt to describe the energy dissipation during frictional sliding.

Historical Developments

The Laws of Friction

The Science of *Tribology* (Greek *tribos*: *rubbing*) encompasses the study of *adhesion*, *friction*, *lubrication* and *wear*. All of these rate dependent processes are dissipative in nature. They involve interfaces that are transient. While adhesion studies are concerned with the formation and destruction of interfaces involving motions normal to the interface, friction studies concentrate on lateral motions of adjacent surfaces in contact. One very important aspect of friction studies has been the behavior of the third medium, referred to as lubricant. In contrast to lubrication that typically concentrates on fluid media (the exception are solid lubricants), wear is the visual manifestation of plastic deformations in solid material that occur in the course of dynamic contact.

Leonardo da Vinci (1452-1519)) can be named as the father of modern *Tribology*. He studied a wide variety of subtopics form friction, lubrication and wear, to bearing materials and geometries, gears, screw-jacks, and rolling-element bearings. About 150 years before *Amontons' Laws of Friction* were introduced, he had already recorded them in his manuscripts. Hidden or lost for centuries, Leonardo da Vinci's manuscripts were found in Spain a quarter of a millennium later.

To the pioneers in *Tribology* one counts besides Leonardo da Vinci, Guillaume Amontons (1663-1705), John Theophilius Desanguliers (1683-1744), Leonard Euler (1707-1783), and Charles-Augustin Coulomb (1736-1806). These pioneers brought *Tribology* to a standard that is still in use today. Some of their findings are summarized in the following three laws:

1. The force of friction, F_F, is directly proportional to the applied load L, i.e., $F_F = \mu L$ with the friction coefficient μ. (Amontons' first law)
2. The force of friction is independent of the apparent area of contact A, i.e., $F_F \neq f(A)$. (Amontons' second law)
3. Kinetic friction is independent of the sliding velocity v, i.e., $F_F \neq f(v)$. (Coulomb's law)

These three laws were attributed to dry friction only, as it has been well known since ancient times that liquid lubrication modifies the tribological properties significantly. Over the past decades, these three laws have been challenged, and found to apply only within limitations. As such, their universality has to be revoked.

The Hydrodynamic Theory of Friction and Beyond

Lubrication, one of mankind's oldest engineering disciplines, was the first tribological discipline for which an effective theoretical basis was developed. These first theories date back to the nineteenth century, starting with Nikolai Pavlovich Petrov (1836 – 1920), Beauchamp Tower (1845 – 1904) and Osborne Reynolds (1842 – 1912), and culminating in the hydrodynamic description of lubrication.

During the first industrial revolution in the nineteenth century, lubricants became increasingly important in ball and journal bearings. Petrov (1883), Tower (1883), and Reynolds (1886) established that the liquid viscous shear properties determine the frictional kinetics. Reynolds combined the pressure-gradient driven *Poisseuille flow* with the bearing surface dictated *Couette flow* assuming, based on Petrov's law (Petrov (1883)), a no-slip condition at the interface between the lubricant media and the solid interfaces. This led to the widely used linear relationship between friction and velocity $F_F(v)$, for a given lubricant thickness D of viscosity η,

$$F_F \propto \frac{v\eta}{D}. \tag{1}$$

Reynolds' hydrodynamic theory of lubrication can be applied to steady state sliding at constant relative velocity and to transient decay sliding (i.e., when sliding is stopped from an initial velocity v and a corresponding shear stress τ_o), which leads to the classical Debye exponential relaxation behavior for the shear stress,

$$\tau = \tau_0 \, exp\left(\frac{-D}{A\eta}t\right); \quad \tau_0 \equiv \frac{F_F}{A} \propto \frac{v\eta}{D}. \tag{2}$$

where A the area of the slider. Note, with the second expression in Eq. 2, we assumed the shear stress to be equivalent the friction-area ratio, as introduced by Bowden and Tabor later. Equation (2) is very important and has been widely ignored by tribologists, even today. The inverse of the ratio $D/A\eta$ represents a material system response time (or relaxation time). It manifests how fast the material can respond to external disturbances. As long as external disturbances are slow in respect to material internal response times, the friction force varies linearly with velocity. The linearity breaks however down when the time scale of the disturbance becomes comparable to the systems relaxation time. While this is a very important point, the tribologists have more or less ignored it, and focused their attention regarding lubricated friction to normal pressure forces and velocity and their impact on the lubrication thickness, which led to the famous Stribeck Curve (1902), Figure 1.

The empirical Stribeck curve reveals that Reynolds' steady state equation of fluid film lubrication is valid for *hydrodynamic lubrication* of thick films (> μm). The hydrodynamic theory breaks however down below a critical thickness threshold at which one has to consider that the sliding material itself is deformed. Assuming elastic deformation of the slider material, the elasto-hydrodynamic lubrication (EHL) theory

(1949) was introduced by Ertel, Grubin, Dowson and Higginson. This theory has dominated the progress in understanding lubrication classically. Refinements have primarily focused on the slider elastic/plastic properties, roughness and the complexity of drainage when the lubricant enters and leaves the contact zone. Only recently (Seiciu and Pavelescu, 2006) the EHL classical theory has been extended to consider also viscosity changes within lubricants. Observing a hysteresis that was attributed to the liquid rheology, lubricants were considered to shift from initially newtonian fluids that exhibit linear stress-strain rate relationships, to quasi-solids with elasto-plastic properties similar to elastomers.

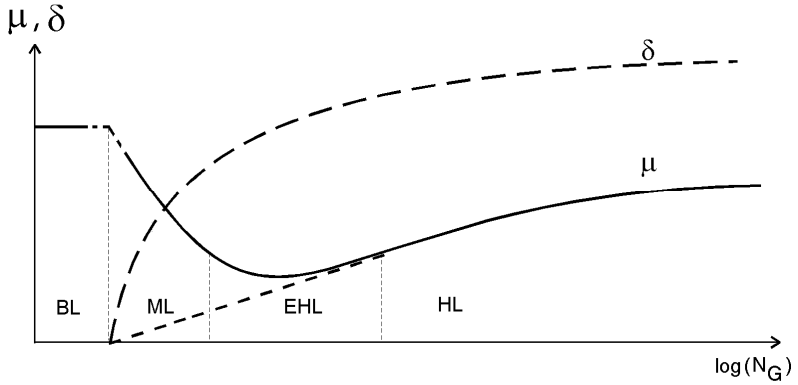

Fig. 1: Stribeck Curve (schematic) relates the fluid lubricant thickness, δ, and the friction coefficient μ to the Gumbel Number $N_G = \eta\,\omega P^{-1}$; i.e., the product of the liquid bulk viscosity, η, the sliding speed (or more precisely the shaft frequency), ω, and the inverse of the normal pressure, P. BL: Boundary Lubrication, ML: Mixed Lubrication, EHL: Elastohydrodynamic Lubrication, HL: Hydrodynamic Lubrication.

The notion that liquids under compression can undergo viscometric changes is not new and has been widely studied by surface forces apparatus (SFA), as early as 1985 by Chan and Horn and 1986 by Israelachvili. From the bulk of SFA work conducted to date, one can infer that newtonian-like liquids can behave, as if they are entropically cooled (i.e., more ordered (structured)). The lubricant thickness length scale over which this "liquid structuring" process could be observed is below 10 nm. In more complex systems (e.g., branched molecules or polymeric containing liquids) no "structuring effect" could be observed in SFA compression experiments.

Returning to the *Stribeck curve* and focusing on very thin films (equivalent to very low sliding velocities) the friction curve reaches a plateau that reflects a solid lubricating behavior, i.e., a velocity independent friction force, as postulated in Coulomb's law. Although, this non-rate dependence of friction at low velocity is rather a manifestation of limitations in macroscopic experiments that are heavily impacted by roughness, incomplete lubricant coverage and wear, it provided one of the first attempts to transition conceptually from lubricated sliding to dry friction. Considering the SFA dedeced molecular model of liquid structuring in ulrathin films, Fig. 2, such a liquid to solid transition is further conceptualized. Representative of the material studied by SFA, Figure 3, provides compression and shear force data, as function of the film thickness, for complex polymeric systems. Notably, the stress- (force) film thickness behavior for complex systems is strictly monotonous, in contrast to the oscillating forces for simple liquids as illustrated in Fig. 2. Over the years, SFA experiments yielded valuable insight

into the shear behavior of a large variety of liquids, thus, providing theoretically the means for molecular engineering of lubricants.

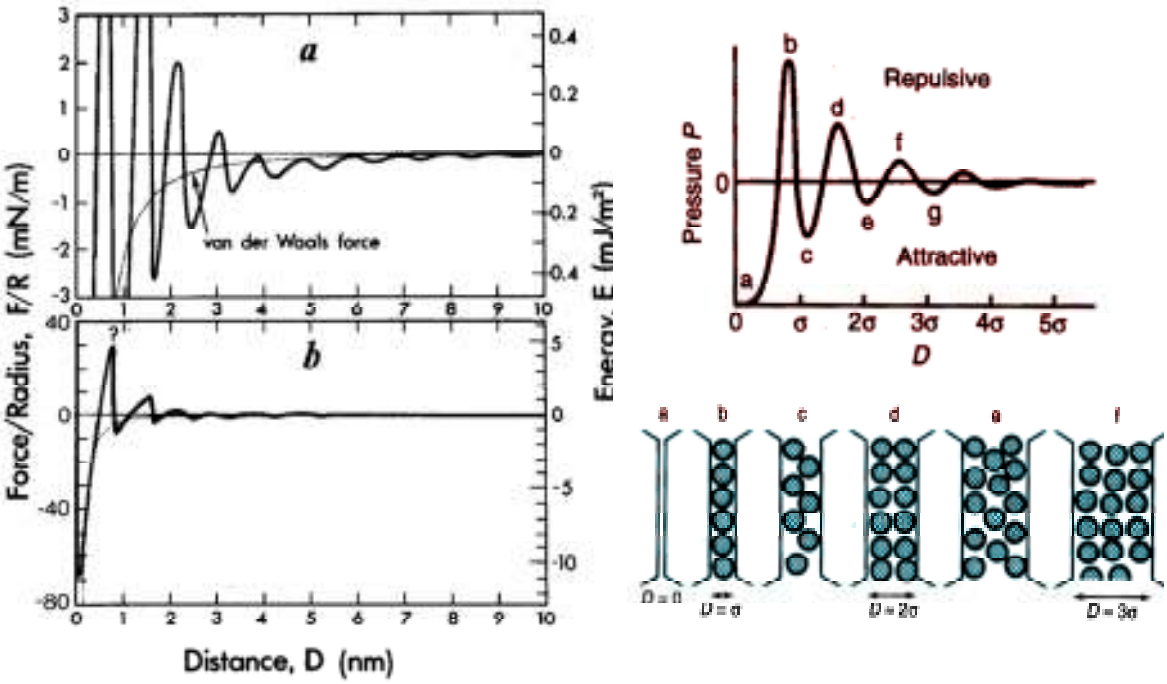

Fig. 2: (*Left*) Oscillatory solvation forces measured by SFA in octamethylcyclotetrasiloxane (OMCTS) as function of OMCTS thickness. (a) Model calculation and (b) experimental data. [Horn, Israelachvili, J. Chern. Phys. 75(3), 1 Aug. 1981]. (*Right*) Visualization of density variation that gives cause for the oscillating forces .

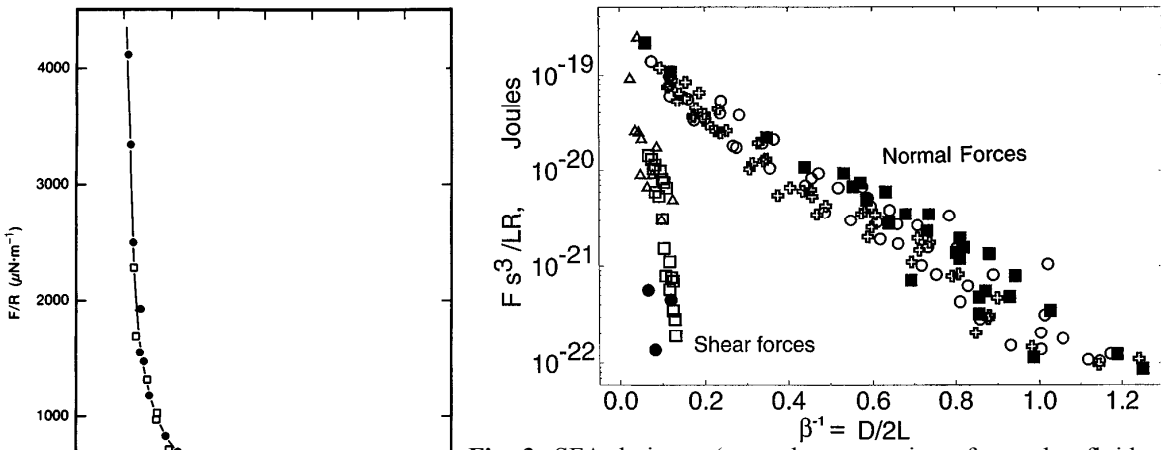

Fig. 3: SFA drainage (normal compression of complex fluids (polymer melts): (*Left*) Perfluorinated polyether (Montfort et al. JPC 88, 7187 (1988)); (*Top*) Polybutadiene (PBD) with a molecular above the limit for entanglements to assure non-newtonian behavior (Klein et al., Nature 370, 634 (1994)).

Solid Contact Friction

Based on the Stribeck curve, in the ultra-low speed regime, called the *boundary lubrication regime*, no hydrodynamic pressure is built up in the lubricant. Consequently the load is carried by contact asperities coated with adsorbed lubricant molecules. This applies to all velocities, if there is no lubricant present, as depicted in Figure 4 below for a dry contact. Boundary lubricants are typically adsorbed layered materials, such as hydrocarbon films (e.g., monolayers of alkanes with surface binding end groups (such as silanes or thiols), molybdenum compounds, and others).

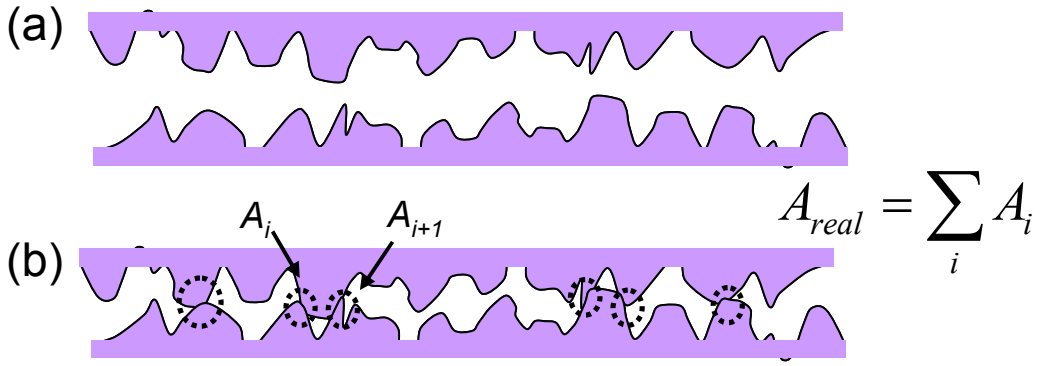

Fig. 4: (a) A representation of two surfaces, rough on small length scales. The two surfaces make contact by touching asperities, forming local contact areas A_i. The real contact area (in contrast to the apparent projected contact area) is given by the sum of the asperity contact areas.

Dry friction and boundary lubrication (we will refer to them in following as *solid (contact) friction*) was considered

(i) geometrically via an interlocking theory by Leonard Euler (1707 – 1783) considering the gravitational potential,
(ii) a thermal fluctuation process in corrugated potential in the 1920th by Ludwig Prandtl (1875 – 1953) and George A. Tomlinson (– 1944),
(iii) a plastic-adhesive process involving asperities in 1954 by F. Phillip Bowden, and David Tabor,
(iv) kinetic activated process of friction based on Eyring's model and proposed by Brian Briscoe and Charles Evans in 1982, and
(iv) a molecular relaxation and mode coupling process in 2003 by René Overney and Scott Sills.

Interlocking Theory

Euler considered the roughness, as the origin of friction. His interlocking theory, which was composed of inclined planes representing the asperities, revealed two terms of solid friction, i.e., static and dynamic (or kinetic) friction. The static friction coefficient is provided by the tangent of the asperity angle, i.e., $\mu = \tan\alpha$, while the dynamic friction coefficient is the reduced static friction coefficient by the kinetic term $2s/gt^2\cos\alpha$, as derived next.

Euler considered theoretically the static equilibrium conditions of a cuboid in contact with an incline plane, Fig. 5 . The normal force $\mathbf{F_N}$, the friction force $\mathbf{F_R}$ are given by the slope $\boldsymbol{\alpha}$ and the weight $\mathbf{F}$ by:

$$F_N = F\cos\alpha$$
$$F_R = F\sin\alpha - F_S$$

with the parallel sliding force $\mathbf{F_S}$.
Per definition the coefficient of friction $\boldsymbol{\mu}$ is the quotient between friction force and normal force and therefore:

$$\mu = \frac{F_R}{F_N} = \tan\alpha - \frac{F_S}{F\cos\alpha}; \quad \alpha \in (0, \frac{\pi}{2})$$

This formal expression represents the static friction as long as $F_S=0$ and the kinetic friction when $F_S\neq 0$. It also results that the kinetic friction is smaller than the static friction. It is worth to note that the analysis is based on a strongly geometrical point of view and does not consider any forces in-between the contact zone nor the real area of contact and any elastic behaviour of the two bodies. In the next analytical step Euler fell back on the *incline plane* experiment of Galilei and set

$$F_s = \frac{2s}{gt^2}F$$

and therefore $\mu = \tan\alpha - \frac{2s}{gt^2\cos\alpha}$ for the kinetic coefficient of friction.

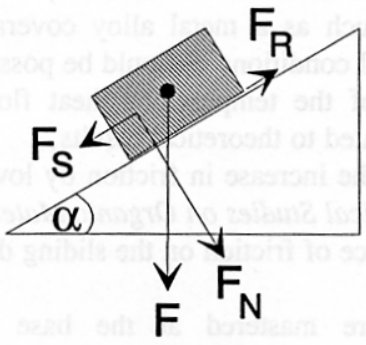

Fig. 5: Inclined plane – representative of an asperity in Euler's interlocking theory.

Friction based on motion within a corrugated energy landscape

One of the enduring challenges in tribology has been to formulate an atomistic and molecular description of energy dissipation in the dry frictional contact zone. By scaling Euler's interlocking theory down to the atomistic scaling, Prandtl and Tomlinson brought forward independently, a instability theory in the 1920th, in which frictional sliding is strictly coupled to thermal vibrations.

The model, illustrated in Fig. 6, is simple. An atom A is moved over the corrugated energy landscape of solid surface. The interaction the atom has with the surface can be anything. While driving relatively the atom, whose connection to its phase is represented by a simple harmonic spring towards one of the atoms in the adjacent corrugated surface, the harmonic parabolic potential is deformed, revealing a local minima. Thus, for an instant during the sliding motion, the atom A is trapped in a local minima away from the equilibrium position, Fig. 6(a). Moving further, the local minima distorts to an inflection point, at which the stuck atom is slipping over the adjacent surface atom into the next corrugation minima, Fig. 6(b). The excess energy it obtained, it releases now in form of vibrations to its solid network. Thus, the resistance to sliding, measured as friction force, is first transferred into local increased potential energy, and then released depressively, into vibrational hearing.

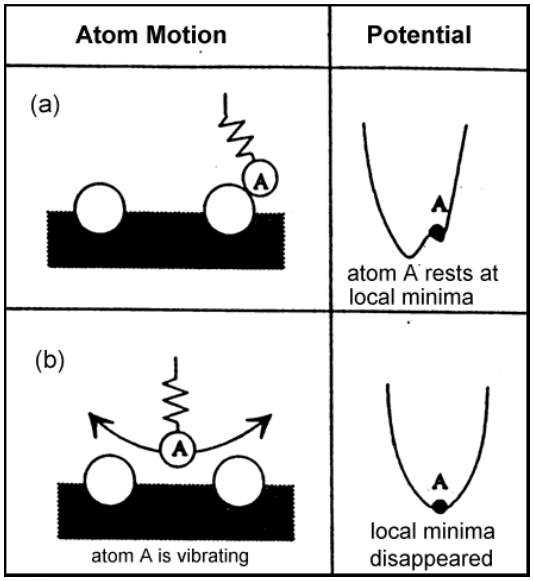

Fig. 6: Prandtl-Tomlinson atomistic model of frictional energy dissipation.

This stick-slip motion has been captured on the nanometer scale on graphite by Mate and McClelland in 1987, and on the truly molecular scale on crystalline lipid film by Overney in 1993, Fig. 7. The latter study shows the friction dependence on the sliding direction, when moving over anisotropic row-like molecular structure.

The one-dimensional Prandtl-Tomlinson model, which has been widely discussed and extended over the past two decades, involves a simple spring that represents the cantilever in friction force microscopy experiment (see illustration in Fig. 7). Thus, the total energy is given by the sum of the surface potential $V(x)$ in driving direction x and the elastic spring potential of the lever, i.e.,

$$E_{tot} = V(x) + \frac{k_L}{2}(x - x_o)^2 , \qquad (3)$$

where k_L and x_o represent the lateral spring constant of the lever, and the symmetry position (absolute energy minimum without sliding), respectively. Typically, models assumed a regular sinusoidal surface potential of the form $V(x) = \sin(2\pi x)$.

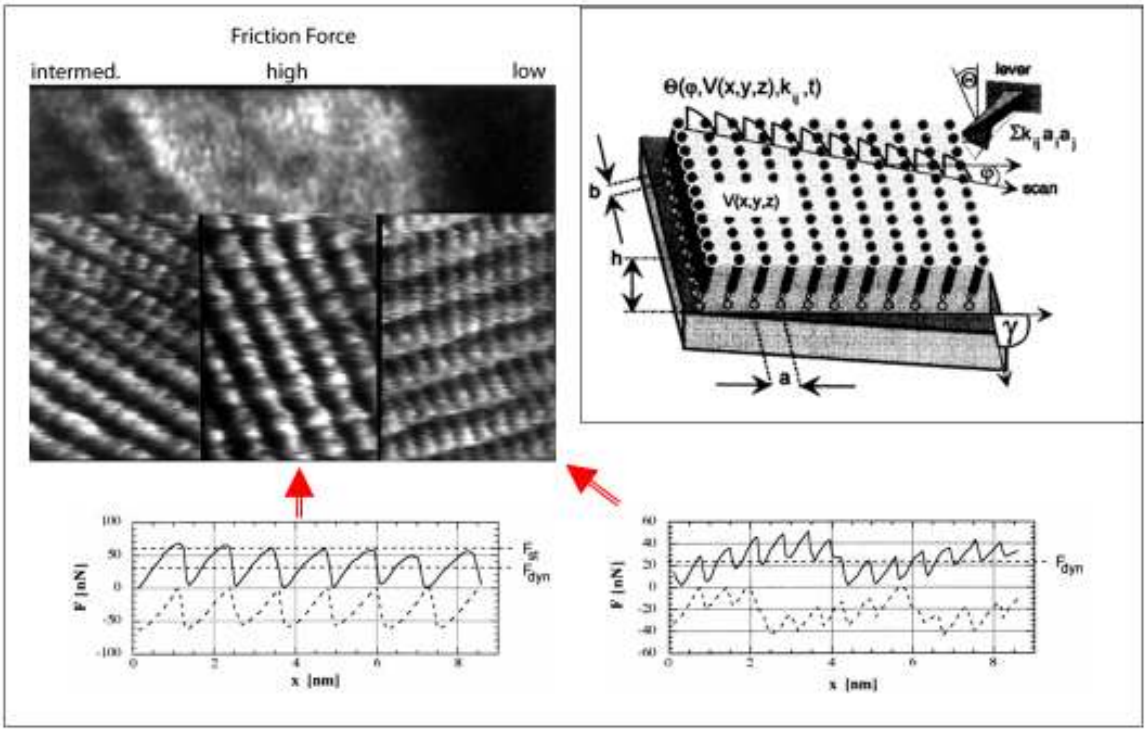

Fig. 7: Stick-slip motion and molecular anisotropy in friction on lipid monolayer (Overney et al., PRL, 72, 3546 (1994)). The lattice anisotropy (row pattern) leads to friction forces on the macroscopic scale that depend on the sliding direction of the nanoprobe. Sliding perpendicular to the rows, i.e., over the most intense molecular corrugation potential, results in highest friction (indicated with bright contrast and strongest stick-slip peaks). Sliding in parallel to the rows reveals lowest friction (dark contrast and small stick-slip peaks).

One aspect that has to be added to this purely mechanical description of friction is a thermal fluctuation term that had led Sang et al. (2001) and Dudko et al. (2002) to express the frictional dissipation behavior with a Langevin equation. The Langevin equation combines the equation of motion (including the sinusoidal potential and perfect cantilever oscillator in the total potential energy E) with the thermal noise in the form of the random force, $\xi(t)$, i.e.,

$$M\ddot{x} + M\beta\dot{x} + \frac{\partial E(x,t)}{\partial x} = \xi(t)\,, \qquad (4)$$

$$\text{where } E(x,t) = \frac{k}{2}\left(R(t) - x\right)^2 - U_o\left(\frac{2\pi x}{\lambda}\right).$$

For the random force, a Gaussian fluctuation-dissipation relation, $<\xi(t)\xi(t')> = 2M\beta k_b T\delta(t\text{-}t')$ was assumed.

Considerations of barrier-hopping fluctuations led to logarithmically dependence of friction on the velocity if the fluctuations were proportionally related to the velocity (Heslot, 1994), or to an exponentially distorted logarithmic friction-*versus*-velocity relationship of the form

$$F_F \propto F_c - \Delta F \left| ln v \right|^{2/3} \tag{5}$$

as found by Sang et al. (2001) and Dudko et al. (2002). Friction force microscopy experiments on solid sodium chloride (NaCl) in vacuum, which exhibited a crystalline surface, and on amorphous polystyrene in a dry nitrogen environment, Fig. 8, exhibited close logarithmic behavior in velocity that were well fitted with either of Heslot's or Sang/Dudko's model. It was pointed out that the small spring constants in atomic force microscopy measurements are responsible for the more pronounced logarithmic behavior of friction in velocity.

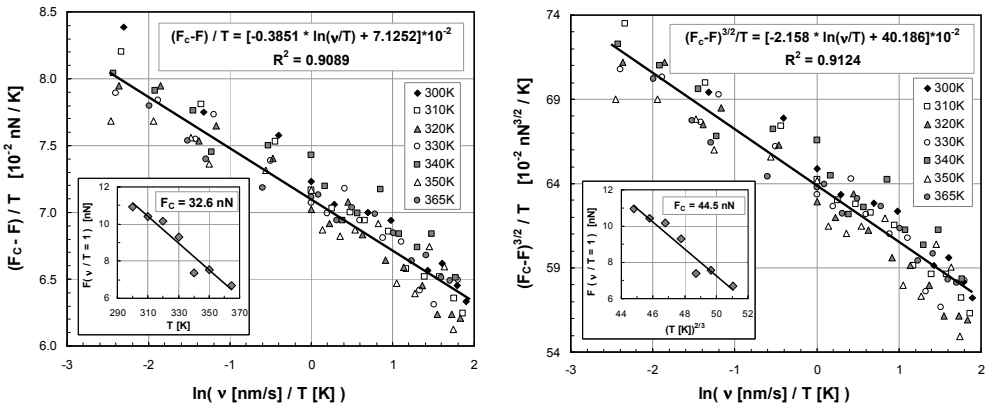

Fig. 8: The difference between a logarithmic (*left*) or distorted logarithmic (*right*) fit of the friction-velocity data on polystyrene was found to be within the error of the data with regression parameters that are very close (Sills and Overney, PRL 91, 095501 (2003)).

Thus, initiated by Prandtl and Tomlinson, the atomistic/molecular stick-slip model revealed theoretically a logarithmic (or close logarithmic) behavior of friction on velocity for solid contact friction, assuming a rigid and regularly repeating surface potential. Clearly, it defies Coulomb's law, and distinguishes itself from the linear viscous behavior found for lubricated surfaces. Interesting, and at the current stage in this text troublesome, is that this model also applies to amorphous surfaces, Fig. 8, which lack a well defined regular corrugated surface potential. Thus, the question arises to what degree adhesive properties, i.e., repeated adhesive bond ruptures play a role in friction. This brings us next to discuss friction from an adhesive perspective.

Plastic-adhesive and elastic theory of friction

Adhesion is a term relating to the force required to separate two bodies in contact with each other. Desanguliers (1734) proposed *adhesion* as an element in the friction process, a hypothesis which appeared to contradict experiments because of the independence of friction on the contact area (Amontons 2nd Law). Therefore the tribologists rejected Desanguliers' proposal and devoted their attention to the more geometrical hypothesis of friction, the interlocking theory of mechanical asperities, as dicussed above. The contradiction between the adhesive issue and Amontons 2nd Law cleared up by the introduction of the concept of the *real area of contact* (see Fig. 4). The real area of contact is made up of a large number of small regions of contact, in the literature called *asperities* or junctions of contact, where atom-to-atom contact takes place. Bowden and Tabor (1954) showed that the force of *static friction* between two

sliding surfaces is strongly dependent on the real area of contact. A very important outcome of their work, which led to the adhesive asperity contact theory of friction, is their detailed discussion about *adhesive wear*. In contrast to abrasive wear which applies to the form of wear arising when a hard, rough surface slides against a softer surface, in adhesive wear, asperity junctions plastically deform above a critical shear strength, which depends on the adhesive forces of the two surfaces in contact. Assuming during a frictional sliding process a fully plastic flow situation of all asperities, friction is found to change linearly with the applied load as demanded by Amontons 1st Law.

Within Bowden and Tabor's simple mechanical adhesive model, it is assumed that all points of contact (asperities) deform plastically during sliding. Thus, the laterally imposed shear force for sliding ("friction force") represents a critical force necessary for sliding to occur under given external conditions, such as load, sliding rate and termpature. Thereby, the imposed shear stress τ (i.e., the lateral force per unit area) is balanced, as per Bowden and Tabor, by the material intrinsic shear strength, τ_s, i.e.,

$$\tau = \tau_s = \frac{F_F}{A}. \tag{6}$$

This assumed balance has to be taken with a grain of salt, as it raises the friction coefficient (defined below) to a material property, which is not the case. The friction coefficient, as we will see is a transport property. It depends on the rate and the velocity, and can also depend on the load.

Returning to Bowden and Tabor's plastic adhesive friction model, we will express the shear strength in terms of the applied pressure P in the contact zone, as

$$\tau_s = \tau_o + \alpha P, \tag{7}$$

and with it introduce the material specific constant τ_o and α, as provided for monolayer fatty acid systems in Table 1. By combining Eqs 6 and 7, and introducing the normal force $F_N = PA$, which is comprised of the applied load and the adhesion force, the friction force is linearly related to the normal force (load), i.e.,

$$F_F = \tau_s A = (\tau_o + \alpha P)A, \tag{8}$$

and thus,

$$F_F = \left(\tau_o + \alpha \frac{F_N}{A}\right)A = \tau_o A + \alpha F_N. \tag{9}$$

Note that α is equal to the friction coefficient μ, if we define it as

$$\mu \equiv \frac{d}{dF_N} F_F, \tag{10}$$

which is as per Bowden and Tabor's model equivalent to

$$\frac{d}{dL}(\tau_o A + \alpha F_N) = \alpha, \tag{11}$$

Bowden and Tabor's plastic model of friction corresponds to Amontons' law which is recovered for most systems, as the pressure induced shear strength component, αP, dominates the zero-pressure shear strength component τ_o in materials. However, in ultrathin films as provided in Table 1, very small α values have been found resulting in nearly pressure independent friction forces, i.e., very low (close zero) friction coefficients.

Table 1: α, τ_o values of fatty acids $(C_{n-1}H_{2n+1})COOH$

	n = 14	n = 18	n = 22
α	0.034	0.038	0.036
τ_o	0.6	0.6	2.2

Source: B.J. Briscoe et al., Proc. R. Soc. Lond. **A 380**, 389 (1982)

Bowden and Tabor utilized the yield stress Y (critical stress above which the linear relationship between stress and strain break down) to express the friction coefficient. From contact mechanics it is known that solids flow plastically at critical mean contact stresses (pressures) $p_{m,crit}$ that are close to three times the yield stress Y (more precisely, when $p_{m,crit} \cong 2.8$ Y). Bowden and Tabor assumed that at this stress, kinetic friction occurs. Consequently the friction coefficient can be expressed as the ratio between the shear strength of the softer material and about three times the yield pressure; i.e.,

$$\mu_{kin} = \frac{F_F}{F_N} = \frac{\sigma_{crit} A_r}{p_{m,crit} A_r} = \frac{\sigma_{crit}}{p_{m,crit}} \approx \frac{\sigma_{crit}}{2.8Y}.$$

Notice that Bowden and Tabor's inelastic adhesive theory provides a constant kinetic friction coefficient as proposed by Amontons.

In contrast to Bowden and Tabor, John F. Archard (1953) suggested friction can also occur if the asperities are only elastically deformed. Utilizing the same equation as Bowden and Tabor (see above, with the exception that the shear stress τ is used instead of the compression stress σ) and combining them with the *Hertzian Elastic Theory* to express the size of the contact, the friction force was found to be proportional to the 2/3-power of the load F_N, i.e.,

$$F_F = \tau\pi\left(\frac{3}{4}\frac{R}{E^*}\right)^{2/3} F_N{}^{2/3}. \qquad (12)$$

Archard's model has been experimentally confirmed in SFM single asperity experiments. The contradiction with Amonton's linear friction-load law is resolved if one considers a loading dependent asperity number distribution. With the inception of the *atomic force microscope (AFM)* and *friction force microscope (FFM)* Archard's elastic theory could be experimentally verified, as illustrated in Figure 9.

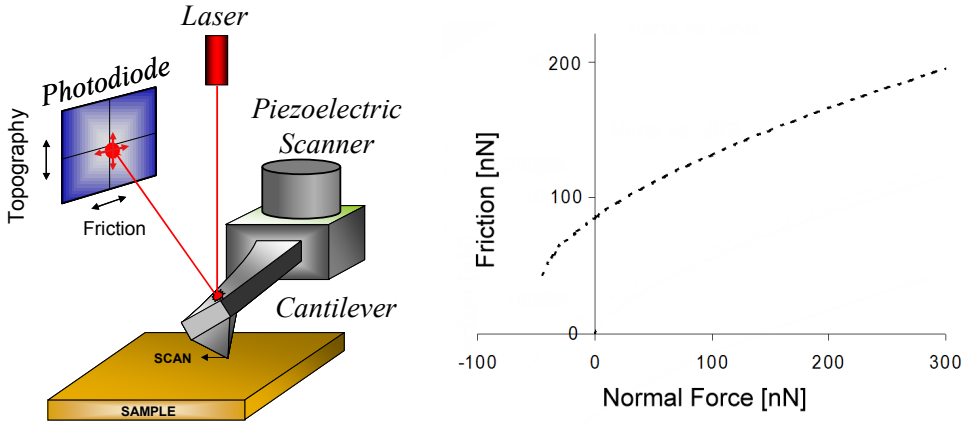

Fig. 9: Non-linear load behavior of fricion found on fatty acids by friction force microscopy.

Some Background on Adhesion and Surface Energies

A very important concept that Bowden and Tabor brought into the discussion of friction are adhesive interactions, which can be perceived as steady bonding/unbinding reactions during steady sliding. The energy of adhesion (or just *adhesion*), W'', i.e., the energy per unit area necessary to separate two bodies (1 and 2) in contact, defines the interfacial energy γ_{12} as, $W'' = 2\gamma_{12}$; $\gamma_{12} = \gamma_1 + \gamma_2 - 2\sqrt{\gamma_1\gamma_2}$, where γ_i (i= 1,2) represent the two surface energies (see Table 2). Assuming two planar surfaces in contact, the Van der Waals interaction energy per unit area is

$$W_1(D) = \frac{-A_{Hamaker}}{12\pi D^2}$$

that is obtained by pairwise summation of energies between all the atoms of medium 1 with medium 2. The Hamaker constant $A_{Hamaker}$ was originally introduced as the product of the molecular (atomistic) number densities in the two solids. To separate two planar surfaces, one has to overcome the energy difference

$$\Delta W = W(D_o) - W(D=\infty)$$
$$= -\frac{A_{Hamaker}}{12\pi D_o^{\,2}},$$

where D_o *is* the material distance in contact, which is surprisingly universal. D_o is known as contact distance, and has been found to be around 0.16 nm for many non-polar materials.

Table 2: Surface energies based on Lifshitz theory and experimental values. (Source: intermolecular & Surface Forces, J. Israelachvili, Academic Press). $A \equiv A_{Hamaker}$.

		Surface Energy, γ (mJ/m^2)	
Material	**A**	**Lifshiz Theory** $A/24\,\pi\,D_o^2$	**Experimental***
	(10^{-20})	{D_o=0.165nm}	(20°C)
Liquid helium	0.057	0.28	0.12 - 0.35(at 4-1.6K)
Water	3.7	18	73
Acetone	4.1	20.0	23.7
Benzene	5.0	24.4	28.8
CCl_4	5.5	26.8	29.7
H_2o_2	5.4	26	76
Formamide	6.1	30	58
Methanol	3.6	18	23
Ethanol	4.2	20.5	22.8
Glycerol	6.7	33	63
Glycol	5.6	28	48
n-Pentane	3.75	18.3	16.1
n-Hexadecane	5.2	25.3	27.5
n-Octane	4.5	21.9	21.6
n-Dodecane	5.0	24.4	25.4
Cyclohexane	5.2	25.3	25.5
PTFE	3.8	18.5	18.3
Polystyrene	6.6	32.1	33
Polyvinyl chloride	7.8	38.0	39

The Hamaker constant can be determined via the Lifshitz theory. It is a continuum theory which neglects the atomic structure. The input parameters are the dielectric constants, ε, and refractive indices, n. The Hamaker constant for two macroscopic phases 1 and 2 interacting across a medium 3 is approximated as:

$$A_{Hamaker} \approx \frac{3}{4} kT \left(\frac{\varepsilon_1 - \varepsilon_3}{\varepsilon_1 + \varepsilon_3} \right) \left(\frac{\varepsilon_2 - \varepsilon_3}{\varepsilon_2 + \varepsilon_3} \right) + \frac{3h\upsilon_e}{8\sqrt{2}} \frac{\left(n_1^2 - n_3^2\right)\left(n_2^2 - n_3^2\right)}{\sqrt{\left(n_1^2 + n_3^2\right)}\sqrt{\left(n_2^2 + n_3^2\right)}\left\{\sqrt{\left(n_1^2 + n_3^2\right)} + \sqrt{\left(n_2^2 + n_3^2\right)}\right\}}$$

where ν_e is the absorption frequency (e.g., for H_2O: $\nu_e = 3 \times 10^{15}$ Hz). Table 3 provides non-retarded Hamaker constants determined with the Lifshitz theory (*c.f.* eq. above).

In general, there is an attractive VDW interaction for $A_{Hamaker} > 0$, and the two macroscopic phases are attracted to each other. In cases where it is desired to have repulsive forces, the medium must have dielectric properties which are intermediate to the macroscopic phases. Consequently, by appropriate selection of the field parameters the adhesion force can be altered, and thus, friction influenced.

Table 3: Non-retarded Hamaker constants in (J) for two interacting media across a vacuum (air)[1]

Medium	Dielectric constant ε	Refractive Index n	Absorption frequency[a] ν ($10^{15} s^{-1}$)	Hamaker Constant $A_{medium/air/medium}$ (10^{-20})
Acetone	21	1.359	2.9	4.1
Benzene	2.28	1.501	2.1	5.0
Calcium Flouride	7.4	1.427	3.8	7.0
Carbon tetrachloride	2.24	1.460	2.7	5.5
Cyclohexane	2.03	1.426	2.9	5.2
Ethanol	26	1.361	3.0	4.2
Fused quartz	3.8	1.448	3.2	6.3
Hydrocarbon (crystal)	2.25	1.50	3.0	7.1
Iron oxide (Fe_3O_4)		1.97	3.0 est	21
Liquid He	1.057	1.028	5.9	0.057
Metals (Au. Ag, Cu)			3-5	25--40
Mica	7.0	1.60	3.0	10
n-Pentane	1.84	1.349	3.0	3.8
n-Octane	1.95	1.387	3.0	4.5
n-Dodecane	2.01	1.411	3.0	5.0
n-Tetradecane	2.03	1.418	2.9	5.0
n-Hexadecane	2.05	1.423	2.9	5.1
Polystyrene	2.55	1.557	2.3	6.5
Polyvinyl chloride	3.2	1.527	2.9	7.5
PTFE	2.1	1.359	2.9	3.8
Water	80	1.333	3.0	3.7

[a]UV absorption frequencies obtained from Cauchy plots mainly from Hough and White (1980) and H. Christenson (1983, thesis).

Reaction Kinetic Model of Friction

In 1936, Henry Eyring (1901 –1981) used his one year earlier developed *Transition State Theory* to express the viscosity as a reaction kinetic process. The concept is simple. The molecules in the liquids are considered to be "caged" by their neighbors. The kinetic theory assumes that highly dilute "empty spaces" exist into which "caged molecules" can

[1] Source: Intermolecular & Surface Forces, J. Israelachvili, Academic Press

transition. In average one can assume a barrier Q for this transition. This idea was picked up by Duckett, Rabinowitz, and Ward in 1970 and further refined by Briscoe and Evans in 1982, and adopted to describe frictional sliding. The beauty of this kinetic model of friction is that it does neither imply a structured surface, nor prescribes the phase state of the system (i.e., solid or liquid).

Eyring' *Transition State Theory* was initially developed for the description of chemical reactions, but its simplicity lends itself to describing a variety of activated processes. The conventional formulation of the Eyring model for shear events, as introduced by Briscoe and Evans, the frequency of movement for a segment to move from its current condition to an open hole is given as

$$f' = \nu \exp\left(\frac{-E_a}{kT}\right) = \nu \exp\left(\frac{-p\Omega - Q + \tau\phi}{kT}\right) \tag{13}$$

where E_a is the apparent activation energy that accounts, in addition to the intrinsic energy Q for a transitional "jump", also for the energy of shear and normal compression, as depicted in Fig. 10. The frequency ν in Eq. (13) represents the effective vibrational frequency of the mobile unit.

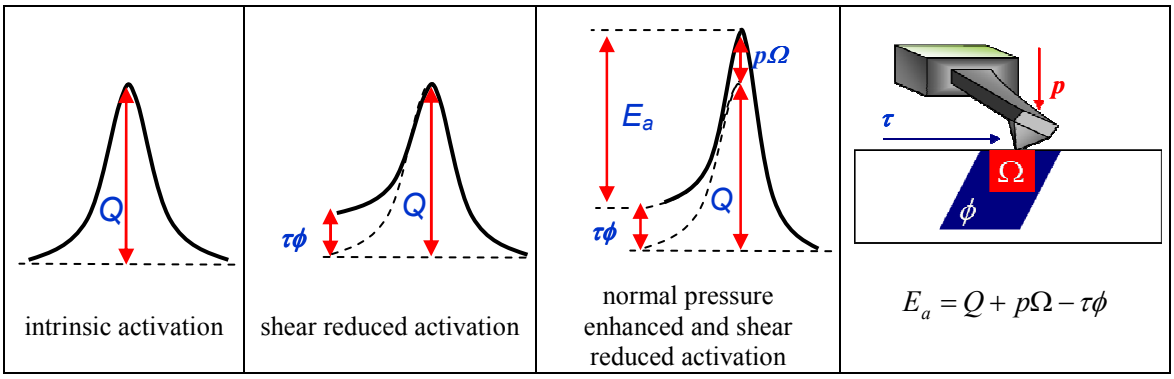

Fig. 10: Eyring reaction kinetic model. The intrinsic activation energy Q is modified by the energy imposed by shear ($\tau\phi$) and pressure ($p\Omega$) to the apparent barrier height $E_a = Q + p\Omega - \tau\phi$. ϕ and Ω represent activation volumes in shear and pressure, respectively, as depicted on the right for an AFM sliding contact.

For cases where the shear stress energy exceeds the thermal noise, i.e., $\tau\phi > kT$, which applies for glassy materials and organic monolayers, the shear stress can be related through Eyring's model to the sliding velocity, v, via the following expression:

$$ln\left(\frac{v}{v_o}\right) = \frac{-Q}{kT} - \frac{p\Omega}{kT} + \frac{\tau\phi}{kT} \tag{14}$$

or

$$v = v_o \exp\left(-\frac{Q + p\Omega - \tau\phi}{kT}\right) \tag{15}$$

where v_o is a characteristic velocity of the system, which is 0.1 m/s and 100 m/s for long chain polymeric glassy systems and organic small molecule self-assembled monolayer systems, respectively, as recently determined by Knorr and Overney. Based on the Eyring cage model, the characteristic velocity v_o can be expressed as $v_o = Cvb$, where

$C \in (0,1)$ is a coupling constant, ν is the jump attempt frequency, and b is the jump barrier distance.

From Eq. (14), one may formulate three sets of equations, in which the shear stress τ can be linearly expressed in respect of the velocity as $\ln(v)$, the temperature T and the normal pressure p, as

$$\tau = \tau_o + \alpha p \,, \tag{16}$$

$$\tau = \tau_o' - \beta T \,, \text{ and} \tag{17}$$

$$\tau = \tau_o'' + \theta \ln v \tag{18}$$

These Eyring expression have been confirmed experimentally by Briscoe in 1982 and repeatedly by other groups (see Fig. 11) involving surface forces apparatus (SFA) and friction force microscopy (FFM) experiments.

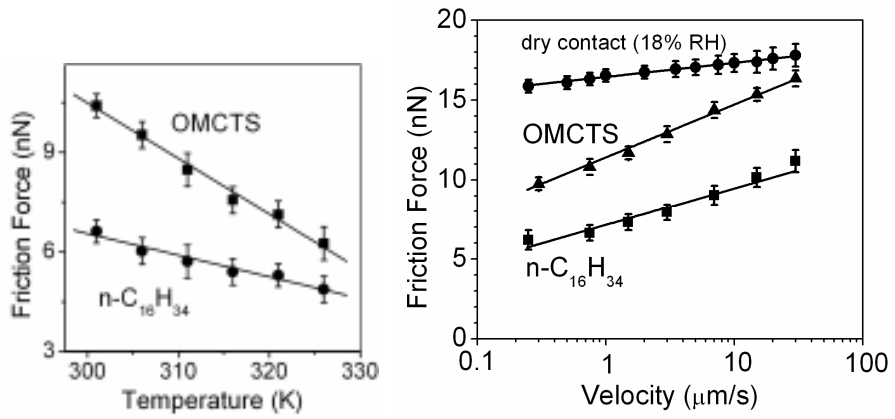

Fig. 11: Friction–temperature and –velocity dependence involving liquids and dry solid contact sliding (He, Overney, PRL 88, 154302 (2002)) confirming the Eyring expressions (Eqs 17 and 18).

Despite the success of the Eyring analysis, it has not become widely used in *Tribology*. The reason is the experimental challenge in quantifying the results, as the real contact area has to be known. Another aspect is that the linear Eyring parameters are approximations that have raised suspicions concerning the interpretation of the data in one or the other experiment. Also the characteristic velocity v_o is not directly applicable from the Eyring analysis, and was often ignored, and the material treated as a fatty acid monolayer, even if this was farfetched. Finally, the Eyring analysis as presented above has a material distinct limitation. It does not work well for systems that relax slowly compared to the slider speed. Hidden in the Eyring analysis is the assumption that the external perturbation (i.e., frictional sliding) is slow compared to material relaxation.

To illustrate how far off the Eyring analysis can be, we show the friction-velocity relationship measured in polymer above the glass transition temperature, a phase that is known to respond sluggishly to stress. In response, an *extended Eyring model* was proposed by Knorr and Overney in 2011, by adding to the Eyring expression of the friction-velocity relationship in its most general form, an additional term (Maxwell term)

that accounts for the time relationship of the external perturbation and intrinsic (internal) material response, i.e.,

$$F_F = \left[\frac{kT}{\phi'} ln\frac{v}{v_o} + \frac{Q}{\phi'} + \frac{p\Omega}{\phi'}\right] + \left[F_o \frac{De}{1+De^2}\right] \text{ with } \phi' \equiv \phi/A, \tag{19}$$

where A is the contact area, and De is the Deborah number, defined as

$$De = \frac{t_t}{t_c} = \frac{v}{v_p}. \tag{20}$$

The Deborah number relates the time of external perturbation, also referred to as the transit time t_t to the characteristic (intrinsic) relaxation time t_c, or in terms of the velocity, the sliding velocity v to the material intrinsic peak velocity v_p, where friction finds its maximum, (see Fig. 12). The peak velocity expresses the material intrinsic relaxation rate. If the external perturbation is comparable or faster the material cannot respond fast enough. In the decaying part of the presented friction-velocity data in Fig. 12, the material lags behind the rate of deformation. The friction reaches its maximum at the "resonance" peak, i.e., when it reaches the relaxation rate (or velocity). In that sense material acts as an energy absorber, and is most effective at rates that match intrinsic relaxation rates.

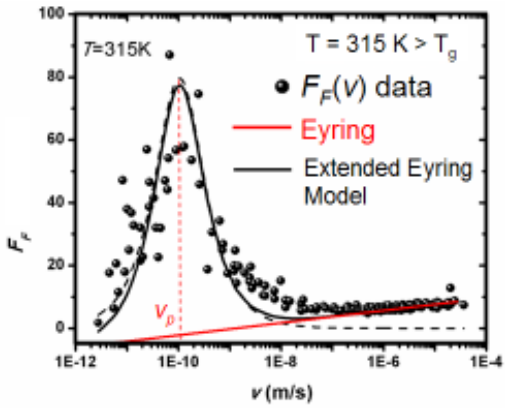

Fig. 12: Eyring model extension considering the interplay between the rate of external perturbation and intrinsic material relaxation. Material: Poly(tert-butyl acrylate) (PtBA) (Knorr, Overney et al., J. Chem. Phys., 134, 104502 (2011)).

Friction a molecular relaxation and mode coupling process

The velocity (or rate) dependence of friction has been discussed for decades due to its highly diverse appearance, Fig. 13. In some work the relationship has been found to be linear in other work logarithmic, or even decaying, and to make matters in even worse, even peaks have been reported, Fig. 12. Many of the explanations provided to explain the qualitative behavior of the curves were hand-waving.

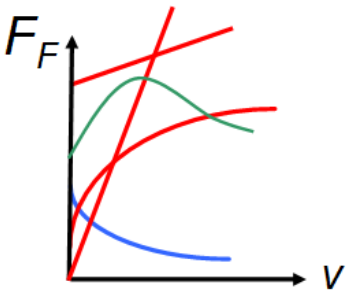

Fig. 13: The diversity of the friction-velocity relationship.

Looking at the theories above, we understand the linear behavior as a viscous behavior and the logarithmic behavior as an activated process. Also the peaks can be understood, if we consider that any material has a limit within which it can respond to

external perturbations.

Consider the experiment illustrated in Fig. 14, on the left hand-side. Note that all data is presented as function of ln(v), as we assume the friction process to entail some sort of an activation barrier that has to be overcome. As every experiment is limited by a range of velocities available, we are reporting within a distinct experimental window of opportunity. Notice, depending on the temperature, the friction curves vary not unlike the curves produced in the open literature for many different materials.

In the 1940s Andrews and Tobolsky treated time and temperature equivalent, and thus, could reach outside their time-window of opportunity, by changing the temperature and with it shift their data accordingly along the time axis. Thus, horizontal shifting of the friction isotherms until they match up and form a continuous line, as illustrated with our data in Fig. 14 on the right hand-side, provides the opportunity to extend the data outside the experimental time-window. The corresponding temperature of the so-called Master curve is therefore dependent on the isotherm that was chosen as the reference data (e.g., T_1) that is not shifted during the process. This procedure is known as the *time-temperature superposition principle*, and is widely used in studying the relaxation behavior of polymers or complex liquids, such as colloids.

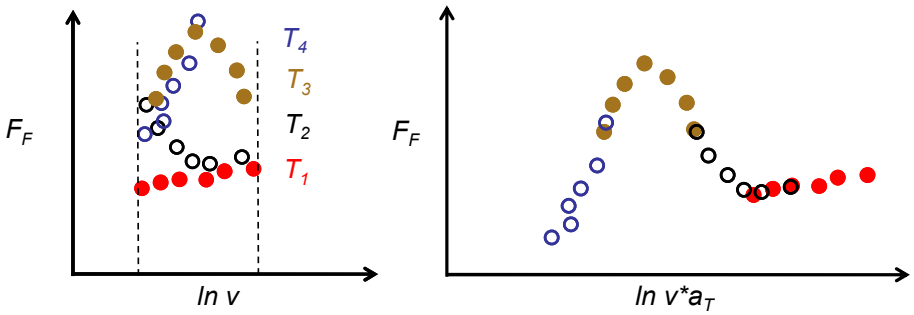

Fig. 14: *(Left)* Friction-velocity isotherms within a set velocity window. (*Right*) The time-temperature superposition principle was applied and the shifted to form a continuous curve (Master curve). The horizontal shift of the data is indicated in the velocity label with the shift factor a_T. The data was also vertically shifted, which is not shown here in the friction label.

The careful reader might have noticed that to obtain the smooth Master curve in Fig. 14, the data had also to be shifted vertically, i.e., in friction direction. As per Knorr, Gray and Overney (2008), the horizontal shift, i.e., the shift factor a_T, as illustrated in Fig. 15, provides the convoluted apparent free energy

$$\Delta G = \Delta H^* - T\Delta S\,, \tag{21}$$

consisting of an enthalpic and entropic energy term, and the vertical shift, Fig. 16, provides a measure of the degree of entropic cooperativity

$$\Delta F_F \propto -\frac{T\Delta S}{\phi'}\,. \tag{22}$$

If the friction process is a truly activated process, then the thermal behavior of the shift factor is Arrhenius, i.e., can be expressed as

$$a_T \propto exp\left(-\frac{\Delta G}{k_B T}\right),$$

When plotted logarithmically versus the inverse temperature, the free energy can be determined from the slope, as illustrated in Fig. 15.

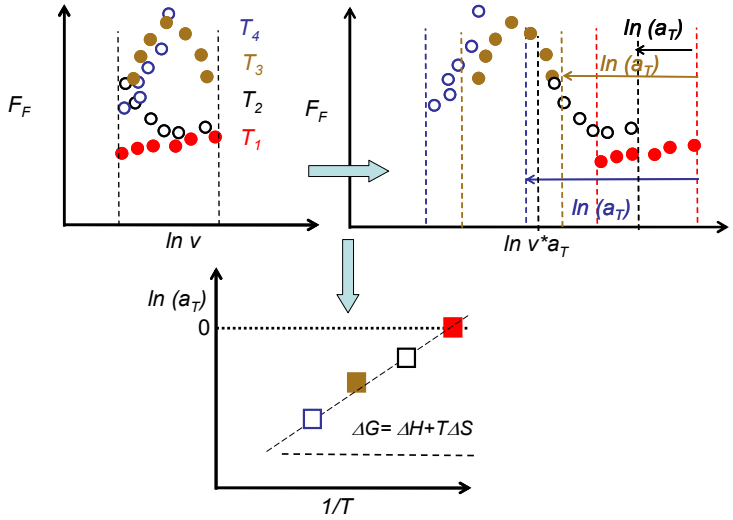

Fig. 15: Illustration of the horizontal data shift only, which yields the shift factors ln(a_T). If plotted as function of the inverse temperature, the shift factors provide the process Gibbs free energy.

As pointed out above with Eq. (21), the free energy $\Delta G = -k_B[\mathrm{d}(\ln a_T)/\mathrm{d}(1/T)]_p$ that is obtained from the slope of the Arrhenius plot (Fig. 15) entails both, an enthalpic and an entropic contribution. If the single activated events are uncoupled, i.e., the process is only enthalpic, ΔG reflects either a material intrinsic activation, or a bonding/debonding energy. If the process involves also cooperativity, i.e., single events (e.g., a molecular chain translation) can only occur in unison with other events (e.g., the translation of neighboring chains), ΔG contains also an entropic component, which can be up to an order of magnitude exceeding the amount of the enthalpic energy. These two possible situations uncouple and coupled events are sketched in Figure 16 for a phenyl side-chain rotations and the translation backbone motion of polymer chain in its matrix, respectively.

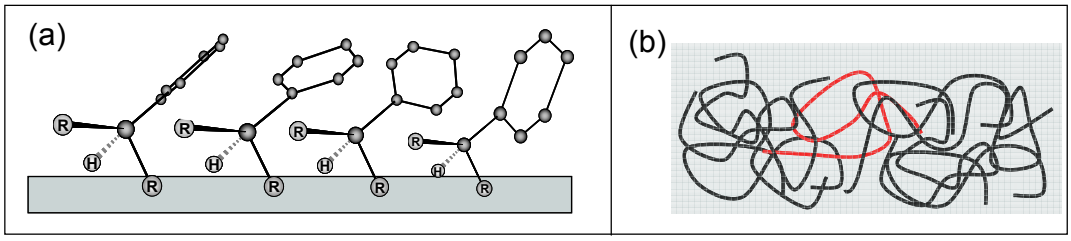

Fig. 16: Illustration of (a) uncoupled side chain rotations, and (b) cooperative translational motion of polymer chains with the matrix.

The degree of entropic cooperativity can be inferred qualitatively from the vertical shifts of the friction data, necessary to obtain a steady Master curve, as illustrated in Figure 16. This shift follows the horizontal shift shown in Fig. 14.

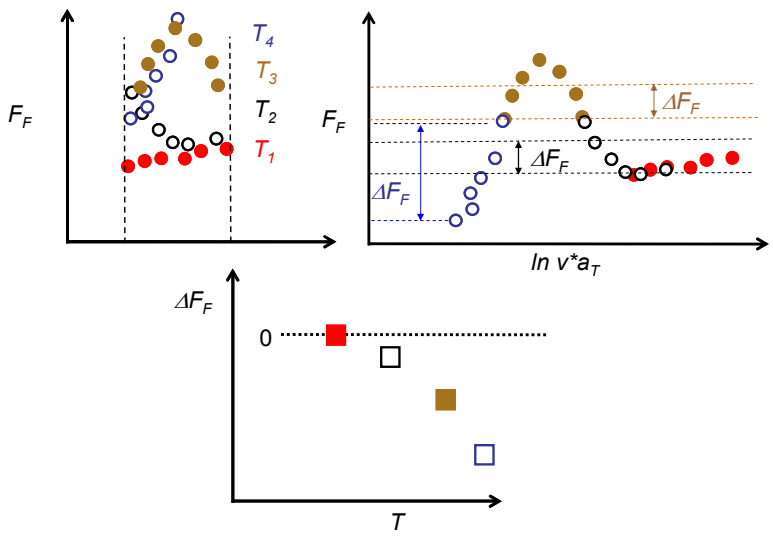

Fig. 16: Illustration of the vertical frictional data shift, which yields the degree of cooperative entropy change in relation to the reference temperature T_1.

To quantify the entropic cooperative contribution, Knorr et al. (2008) used H. Starkweather's reaction kinetics relationship developed in 1988, which yield for the Gibbs free energy

$$\Delta G^* = RT\left[1 + ln\left(\frac{k_B}{2\pi h}\right) + ln\left(\frac{T}{f_p}\right)\right] + T\Delta S^*,$$

It introduces the (peak) frequency of relaxation f_p, and uses the universal gas constant R, and the Planck constant h.[2]

While the peak frequency f_p can be estimated from IFA data, leading to errors within the 5% range, an exact determination requires a spectral analysis that is dependent on the frequency. Frequency spectra, as provided in Fig. 17 (*left*) from dielectric relaxation spectroscopic (DRS) measurements, present if paired with the IFA friction velocity spectra, Fig. 17 (*right*), the unique opportunity to determine the length scale of cooperativity.

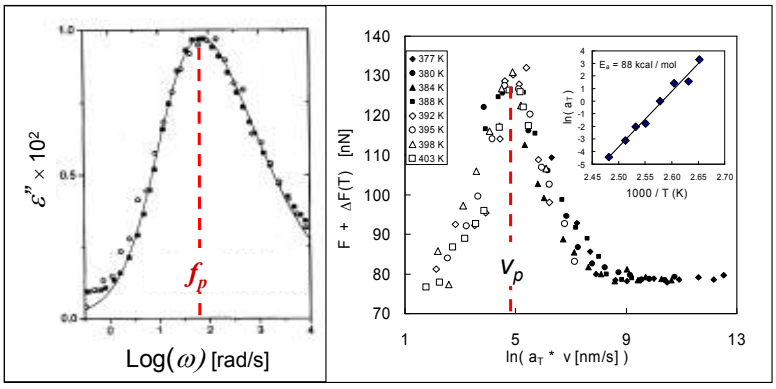

Fig. 17: Illustration of the vertical frictional data shift, which yields the degree of cooperative entropy change in relation to the reference temperature T_1.).[Sills and Overney, J. Chem. Phys. 123, 134902 (2005)]

[2] "*" indicates that the energy is expressed in molar basis.

Overney and Sills recognized in 2005 that the ratio of the two relaxation parameters, f_p from DRS and v_p from IFA, i.e.,

$$\xi \equiv \frac{v_p}{f_p} \tag{23}$$

result in a length scale ξ, which corresponds to the entropic cooperation length in a polymer "melt" above the glass transition temperature, as shown in Fig. 18.

Thus, mode coupling of thermally active modes into the friction signal, which ends up to be a spectroscopic intensity signal, as found for instance in scattering experiments, reveals

- the enthalpic activation energies of the modes in question,
- the mode coupling cooperative entropic behavior, and
- the length scale of cooperativity.

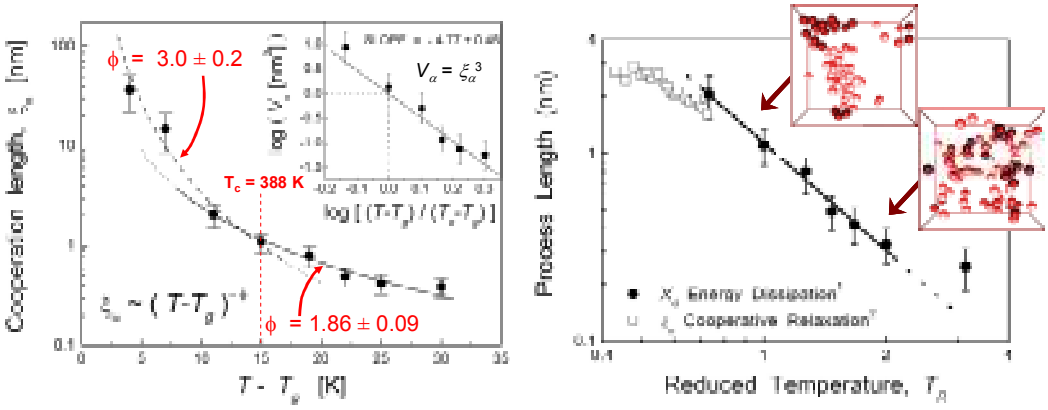

Fig. 18: Cooperation length of the α-relaxation, ξ_α, for polystyrene using DRS and IFA and Eq. (22). The data (left and right) are equivalent just differently presented. The process length is equivalent to the cooperation length. $T_R = (T-T_g)/(T_c-T_g)$ is the reduced temperature, and T_c is the crossover temperature, obtained from friction-temperature curves above the glass transition temperature T_g (see Fig. 20).[Sills and Overney, J. Chem. Phys. 123, 134902 (2005)]

It is clear at this point that the friction signal entails by far more, as it could have ever been anticipated by Amonton's and Coulomb's laws. It also shows us that there is not one particular rate behavior of friction. It depends on the time (velocity) window of observation and the temperature. If the time window is large enough in respect to the sub-molecular or molecular mode, or by artificially generating such a window by employing the time-temperature superposition, the friction-velocity plot reveals a peak that is directly related to the relaxation of the coupling mode, as we have seen.

The frictional mode coupling process of a stylus-like slider with the thermal rotational submolecular modes of a free surface is illustrated in Fig. 19(a). Initially rotations occur randomly with positive or negative spin directions, designated with bright (gray) arrows in Fig. 19(a). The slider shall be moving diagonally over the surface. In its trace it leaves molecules that have interacted it, and are pointed out in red (or darker contrast) in Fig. 19(a). This information exchange of the existence of the slider causes an entropy reduction. The entropy reduction is here visualized in the concerted (negative) rotation of the molecules that have been in contact with the slider. As per the second law of

thermodynamics, any entropy reduction requires outside work. In this case, entropy reduction is the cause for frictional dissipation, i.e., energy has to be supplied to the slider to keep it moving. This model was inspired by the first experimental observation of the phenyl rotation at the polystyrene surface, Fig. 19(b).

If we assume, as a thought experiment (Gedankenexperiment), this to be the only process of frictional dissipation, then one could dissipate energy without the generation of heat. As the rotating sidechains, illustrated in the inset in Figure 8, are connected to the bulk of the systems that possesses vibrational modes, we could spin our thought experiment even further. We could assume that the rotational modes are coupled to the bulk vibrational modes, and thus, initiate a secondary, time-delayed, energy transfer process, in which the rotational modes transfer energy to the vibrational modes by falling back into a disordered entropic rotational state. Having gained vibrational energy, the bulk system has on a macroscopic scale raised its temperature. Thus, this idealized and possible scenario of friction dissipation illustrates that the dissipation process does not have to be directly connected to heat generation. Heat generation can be a secondary process, or not at all occur during frictional sliding. In conclusion, we see that the Prandlt-Tomlinson model and all that followed provide a limited view of friction dissipation.

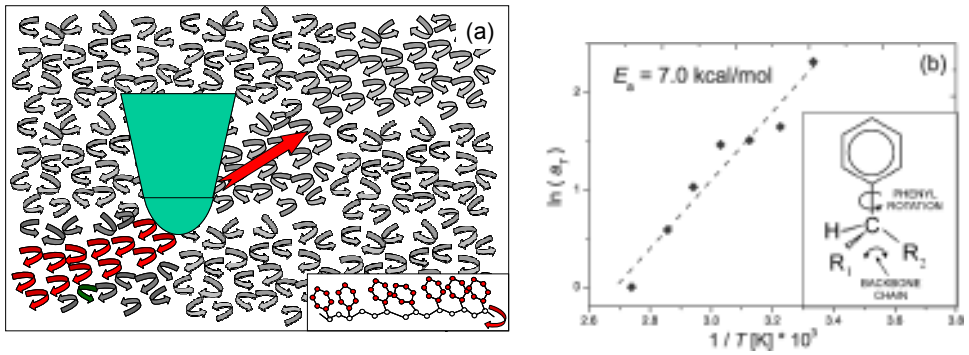

Fig. 19: (a) Visualization of friction mode coupling with active thermal modes. (b) First experimental verification on the phenyl rotation on polystyrene [S. Sills and R.M. Overney, (2003), *Phys. Rev. Lett.* 91(9), 095501, 2003].

Molecular mobility and friction – Energetics vs. friction coefficient

In Figures 17 and 18, we presented IFA and DRS results of polystyrene (PS). To illuminate the temperature and velocity dependence on friction and the friction coefficient, and to get a better understanding on how the molecular properties play into the friction behavior, we will discuss the results obtained on polystyrene a little further.

Materials with high mobility

Polymers above their glass transition are still solids but possess enhanced molecular chain mobility, which translates macroscopically in high mechanical flexibility. In Fig. 20, the friction force and coefficient is shown around the glass transition. The force is strongly dependent on the temperature within the temperature regime of T_g and $T_c \approx T_g + 15$ K, the crossover temperature. This friction behavior coincides with the variation of the cooperation length within the same temperature regime, Fig. 18. Thus, the cooperation length impacts the friction force. Above the crossover temperature T_c, the cooperativity in polymer melts breaks down, as the thermal energy (disturbance) is large enough to interfere with the mutual motion. This results in a temperature independent

behavior of friction above T_c. By rationally designing the molecules, one could control the degree of cooperative motion and T_c, and thus, molecularly engineer material with desired friction properties.

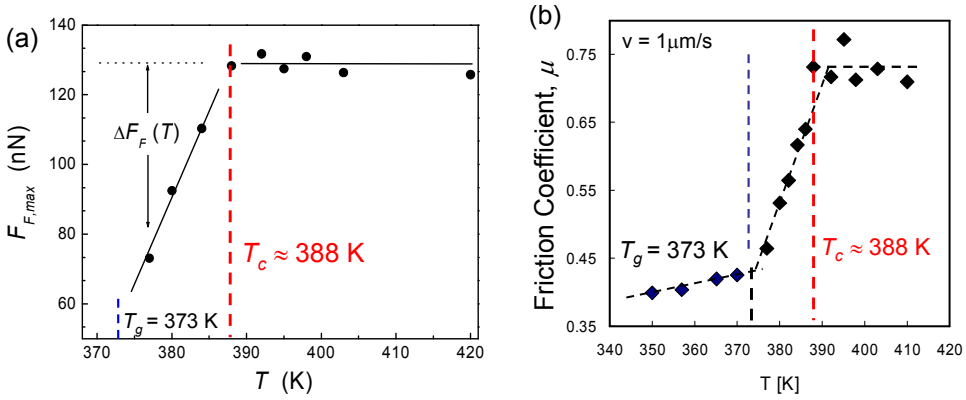

Fig. 20: Friction study of polystyrene. (a) friction force (b) friction coefficient around the glass transition T_g and the crossover temperature T_c [Sills and Overney, J. Chem. Phys. 123, 134902 (2005)].

Materials with low mobility

As the prior discussion was focused on material with high mobility (for polymers above T_g, where the backbones of the polymer chains are mobile), we will focus next on material with low mobility, such as isolated sub-molecular motion (e.g., side-chain rotations), or bonding-debonding events.

Polymer glasses and isolated sub-molecular motion

Above the glass transition of polystyrene, the friction dissipation behavior has been found to be strongly affected by the cooperativity of the thermally active modes. Below T_g, as shown in Fig. 21, the friction force F_F and the friction coefficient $\mu = dF_F/dL|_{T,v}$ are a function of the applied load L (or more precisely, the pressure $p = L/A$). Analyzing these pressure regimes with IFA (comprised in Table 4) reveals two different molecular modes responsible for the disparity in the friction behavior. It is interesting to note from the two coexisting thermal active modes, that is, the side-chain phenyl rotation (γ –relaxation) and the isolated backbone crankshaft motion (β–relaxation), only one couples predominantly with the frictional sliding mode. While at low load the phenyl rotational mode couple with the frictional slider (the phenyls are known to have an increased preponderance at the free polystyrene surface), at higher loads the backbone crankshaft motion becomes accessible by the slider.

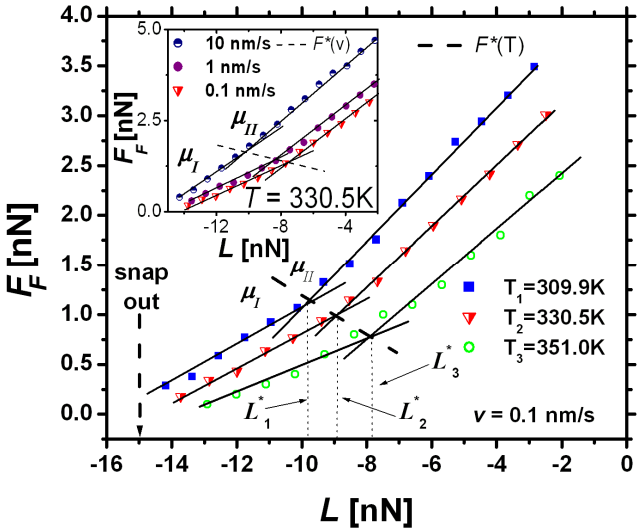

Fig. 21: Friction behavior of polystyrene below the glass transition. [Knorr, Gray, Overney, JCP 129 (7), 074504 (2008)].

Table 4: Molecular origin for frictional dissipation in polystyrene.

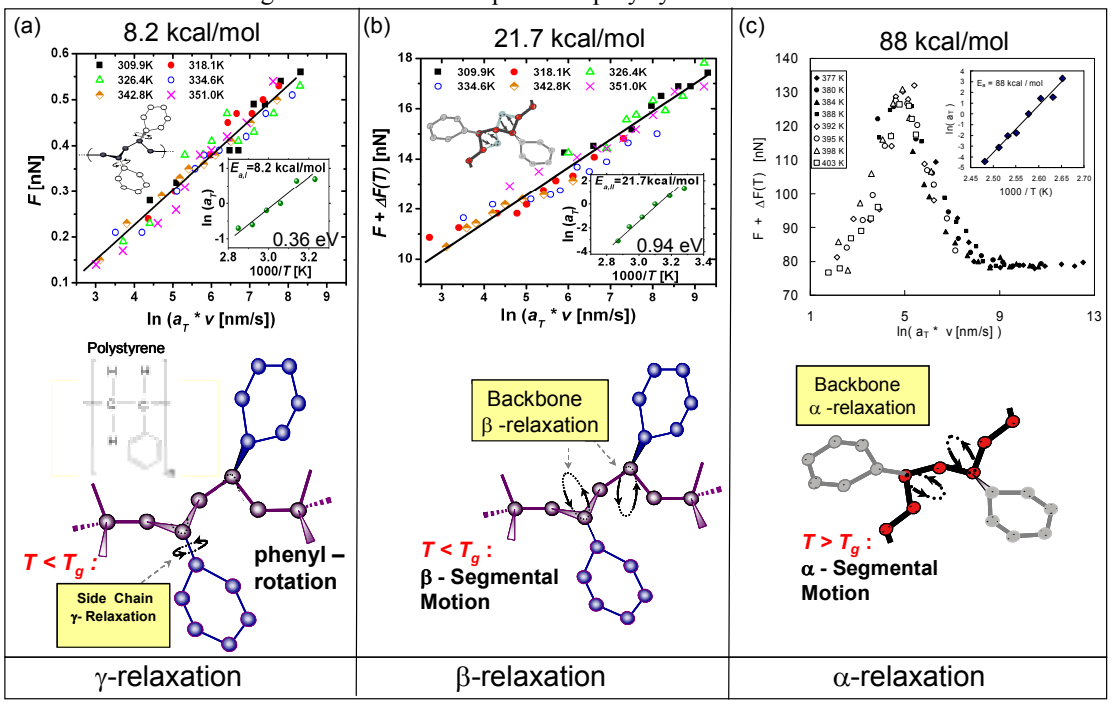

These results show that frictional mode coupling can also depend on the external pressure parameter. This insight highlights the interconnection of molecular properties, load and interfacial area (or roughness). Thus, geometrical (roughness) and contact mechanical considerations that started with Euler's interlocking theory followed by Bowden and Tabor's Hertzian elastic discussion of friction are noticeable also on the molecular scale. The friction defining principle parameters have thereby shifted to pressure, temperature and rate. It is important that by discussing friction, one has to fix two of these parameters, while changing the third one, or establish a combination

parameter; otherwise one travels the phase-diagram in an awkward direction. The analogy is found in thermodynamics, in which one discusses phase diagrams under iso-conditions (e.g, isobaric or isothermal).

Isolated bonding-debonding reactions

As per Bowden and Tabor, one aspect of friction involves adhesion forces. During the relative motion of two finite-sized surfaces in contact, a new interface is constantly formed at the front end, and, at the trailing end the two surfaces are ripped apart. Thus, from a molecular/atomistic perspective, we have to consider bonding-debonding reactions between the two surfaces. It is sensible to assume that the unperturbed reaction kinetics couples with the frictional sliding event, yielding, as shown in Figure 22, a bonding specific energy.

In this particular example (Fig. 22) two molecular *thermal-mode-inactive* materials, i.e, a silicon oxide tip and atomically smooth graphite surface, SiO_x-HOPG, were moved in frictional contact in a dry nitrogen environment. Thus for a SiO_x-HOPG frictional system only bonding-debonding reactions can be held accountable for the measured 0.8 eV, Fig. 22. We note further from linear logarithmic behavior of friction in velocity that the experimental velocity window was slow in comparison to the relaxation time of the interfacial reactions. Additional analysis revealed that the bonding-debonding events were non-cooperative. We can conclude that the interaction that coupled here with the sliding motion is a non-specific dipole-dipole interaction, known as Van der Waals dispersion interaction. Such interactions depend on the dielectric and refractive properties of the materials and the surrounding media (nitrogen gas) involved.

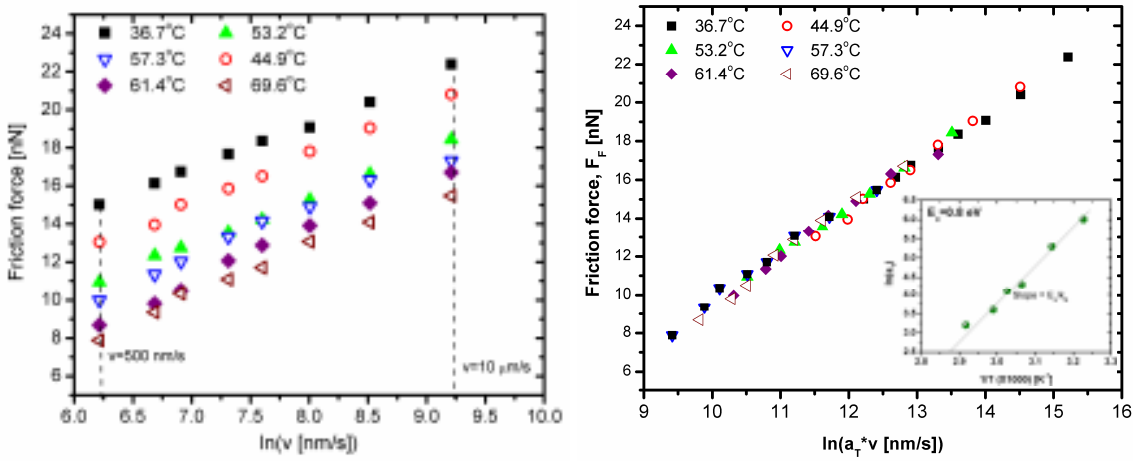

Fig. 22: IFA analysis of graphite (HOPG, highly orientated pyrolytic graphite in a dry < 4% RH nitrogen environment) revealing an activation energy of 0.8 eV. (*Left*) Friction-velocity isotherms. (*Right*) Friction Master Curve.

To expand our view of bonding/debonding interaction, to interaction within the solid system, we consider next molecular systems, where again IFA data can be used to guide molecular engineering. In particular, we will look at molecular glassy chromophores (Fig. 23), which are used in optical modulators. To operate effectively, the molecules in these materials must be aligned, and, once aligned, this alignment must be stable over long periods of time. One way to provide stability is through interactions between the

molecules, in this case between aromatic (i.e., phenyl, naphthyl and anthryl) groups and fluoro-aromatic groups (i.e, pentafluorophenyl) that are dendritically added. These components have quadrupoles that are of similar magnitude, but opposite sign, so they stack in a face-to-face fashion, providing stability, as shown in Fig. 23.

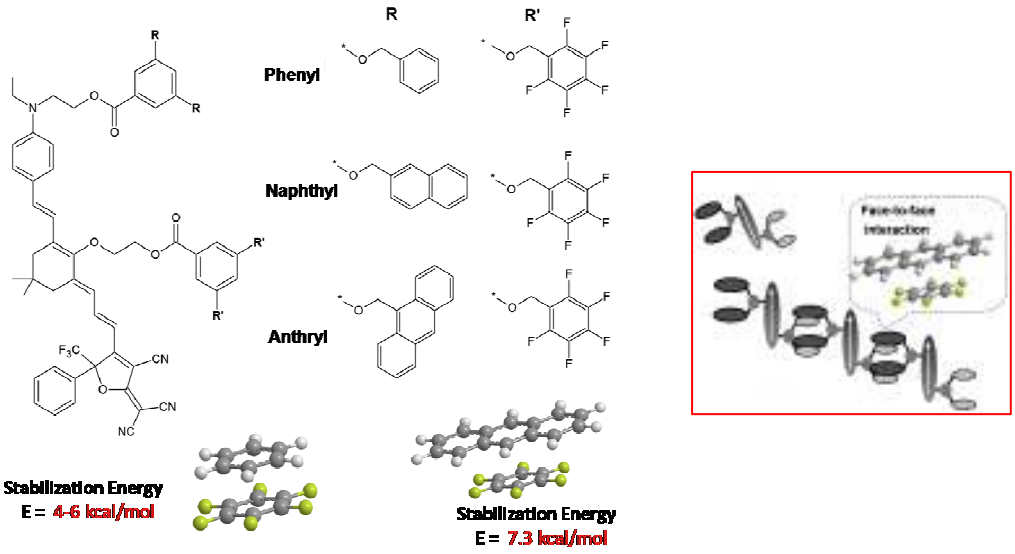

Fig. 23. Glassy chromophores with phenyl, naphthyl, anthryl and pentafluorophenyl groups and associated stabilization energies for the face-to-face (quadrupolar) interactions[19]. *Bordered inset to the right*: Schematic representation of the molecules designed, entailing the chromophores with strong dipole moments (white arrows), and the dendritic pending quadrupolar ("reactive") groups.

IFA results on these materials are provided in Fig. 24. As shown, the master curves (Fig. 24a) show peaks in velocity, while the ln a_T vs. $1/T$ plot (Fig. 24b) shows regions with three distinct slopes, bounded by transition temperatures T_1 and T_2. The slopes clearly show increasing activation energy (therefore increasing stability) for increasing aromatic group size (i.e., from phenyl to naphthyl to anthryl). The vertical shifting plot (Fig. 24c) shows that cooperativity (i.e., vertical shifting) begins just above T_1, and increases with increasing temperature. Cooperativity in this case results from motion of the entire molecule, leading to loss of alignment. Therefore, IFA on these materials has shown that larger aromatic groups provide greater stability, and that the materials should be operated below T_1 to prevent loss of alignment.

We can conclude that bonding/debonding interactions within the material and between the sliding interfaces can turn into thermal active modes that are the dominating modes for friction dissipation. The challenge that remains from a molecular engineering perspective is to come up with *rules of thumbs* that are based on energetic information. For instance, we still do not know, if high or low mode energy is required for small frictional dissipation. We will shine some light on to this aspect in our last paragraph on molecular tribology.

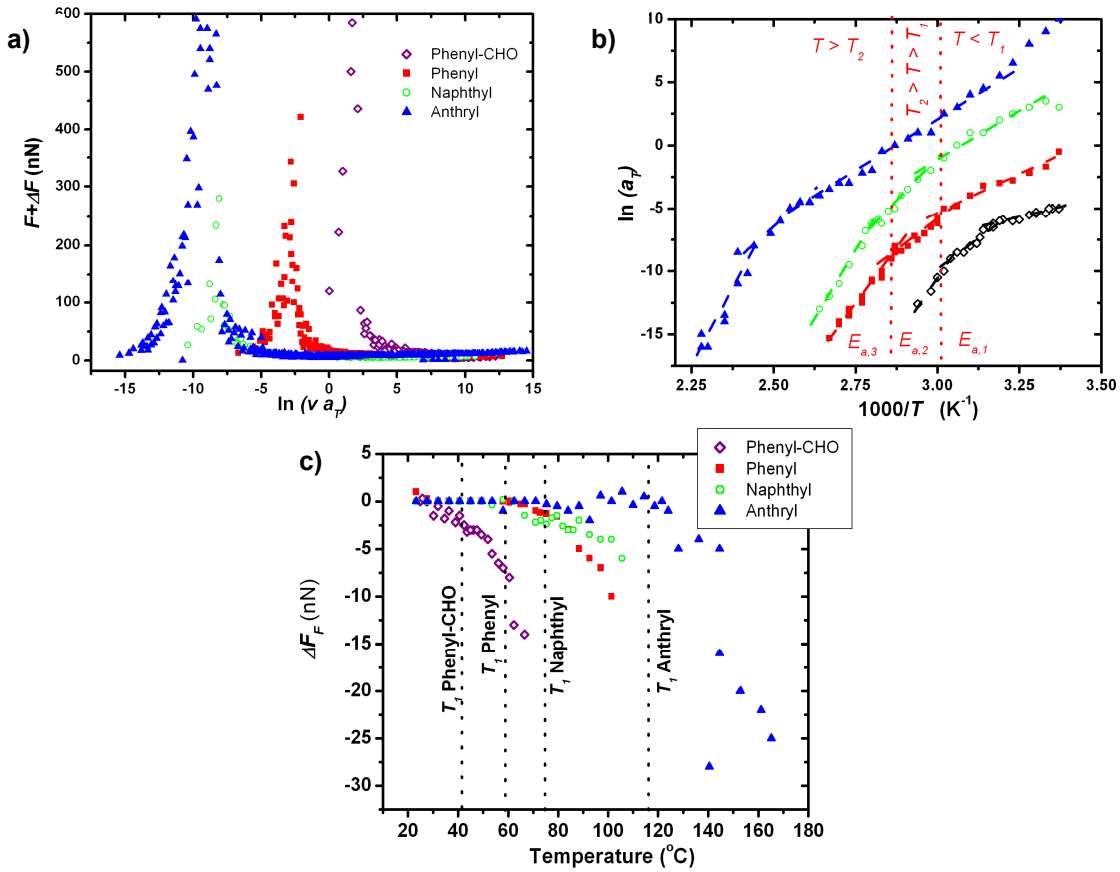

Fig. 24. IFA results for glassy chromophores: (a) master curves, (b) ln a_T vs. $1/T$, (c) vertical shifting as a function of temperature.

Dimensional relationship between friction and mode energy

The friction coefficient, although not truly a property, is from an engineering perspective still the most widely used parameter to express pseudo-quantitatively the frictional dissipation process. We shall first inspect tribological systems that operate mainly two-dimensionally (2D or d = 2), i.e., along a plane, such as atomistic highly structured and stiff systems (e.g., graphite), organic monolayer systems, or solid Van der Waals systems with very weak molecular interactions so that the top surface molecules are easily displaced via shear motions. The energy-friction values of such systems are compiled in Figure 25 connected by a dashed line. We notice for 2D systems, there is a clear trend for lower friction coefficients at higher mode energies. That this trend cannot be generalized to all materials can be seen by adding values for randomly studied polymer systems.

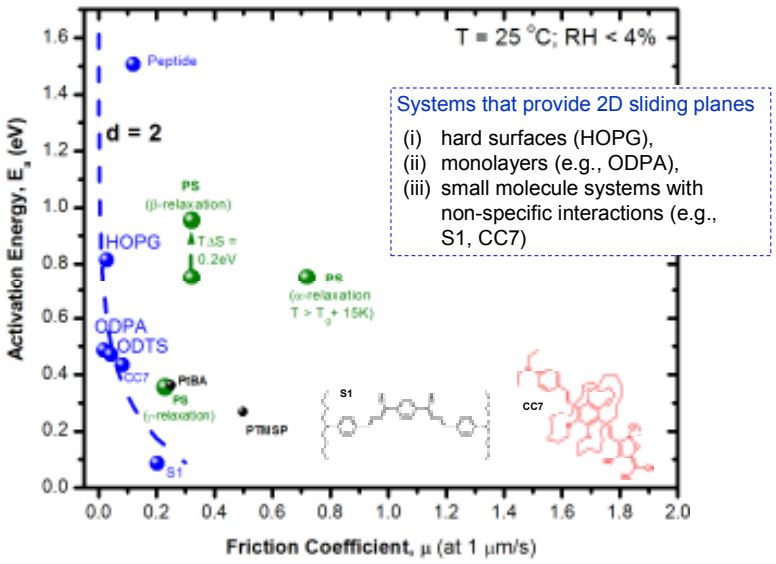

Fig. 25. IFA apparent energies E_a are contrasted to the friction coefficient. While 2D systems reveal a trend (dashed line), no trend can be inferred from uncorrelated complex (polymer) systems.

With the premise that the dimensionality of the momentum transport during the sliding motion provides a material classification to establish fundamental energy-friction relationships, we focus next on three-dimensional (3D or d = 3) systems, namely, the amorphous glasses discussed above. Figure 26 shows a clear trend for these systems that are different quantitatively (i.e., shifted) but qualitatively the same as the 2D systems. An increase in the interaction bonding energy was found to yield a decrease in the friction coefficient. This is equivalent with the phenomenological contact mechanical finding that an increase in the stiffness of the material results in a decrease in the friction coefficient.

Finally, left to show is that this trend also applies to material that behave fractal-like (i.e., between 2 and 3) during a shear behavior. For this purpose, we present the energy-friction coefficient data of a chromophore containing material that uses coumarins (liquid-crystal-like) moieties as dendrons. The liquid-crystal-like dendrons give the material a close planar configuration that was found to be of d = 2.2 dimensionality. Figure 27 reveals that indeed the trend line of such material is qualitatively similar to d = 2, 3 and located in between the planar (d = 2) and bulk (d=3) behaving materials under frictional sliding.

With this we have found a direct relationship between the apparent energy and the friction coefficient, and thus, have the means for rational engineering of molecules towards low friction dissipating interfaces.

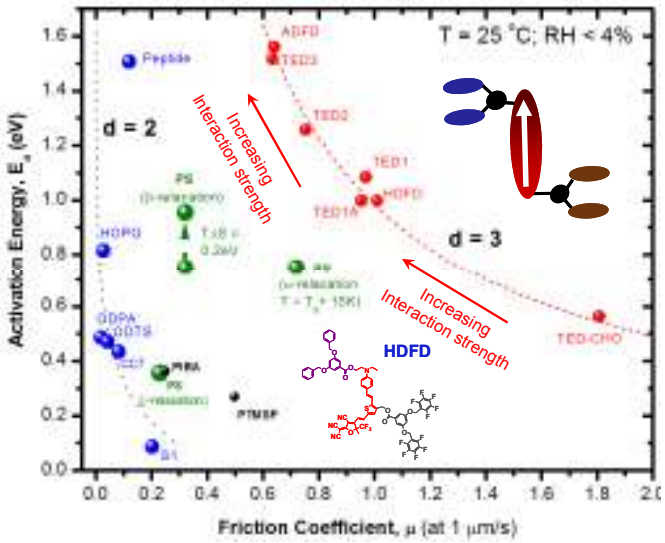

Fig. 26. IFA apparent energies E_a are contrasted to the friction coefficient. The d = 3 molecular glass systems reveal a trend (dashed line), qualitatively similar to the d = 2 systems.

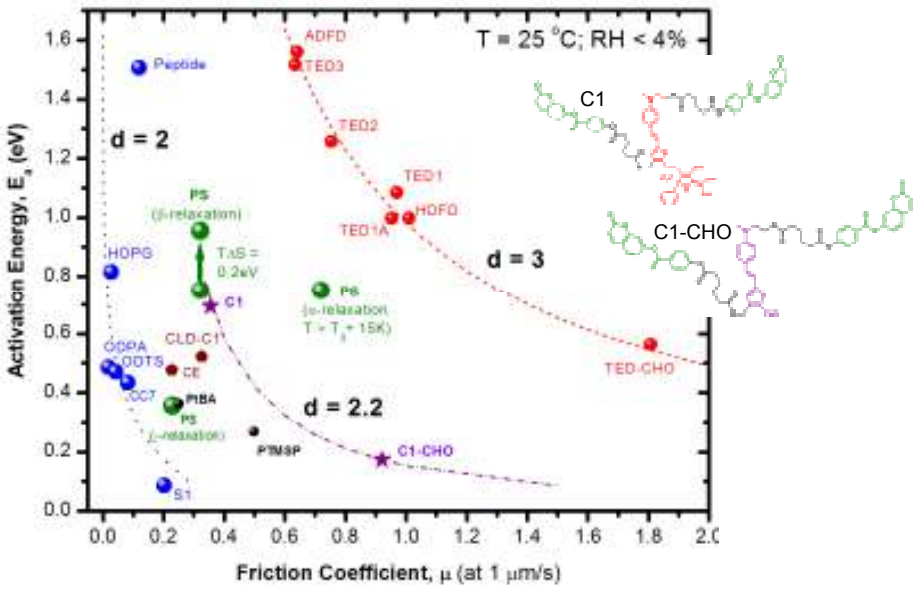

Fig. 27. IFA apparent energies E_a are contrasted to the friction coefficient. The d = 2.2 molecular glass systems reveal a trend (dashed line), qualitatively similar to the d = 2 and d = 3 systems.